Nanoscale Structural and Electronic Properties of Cellulose/Graphene Interfaces

Gustavo H. Silvestre[ID],[1] Felipe Crasto de Lima[ID],[2] Juliana S.
Bernardes[ID],[3,4] Adalberto Fazzio[ID],[2,4] and Roberto H. Miwa[ID][1]

[1]*Instituto de Física, Universidade Federal de Uberlândia, 38400-902, Uberlândia, MG, Brazil*
[2]*Ilum School of Science, Brazilian Center for Research in Energy and Materials (CNPEM), Campinas, SP, 13083-970, Brazil*
[3]*Brazilian Nanotechnology National Laboratory, Brazilian Center for Research
in Energy and Materials (CNPEM), Campinas, SP, 13083-970, Brazil*
[4]*Center for Natural and Human Sciences, Federal University of ABC, Santo André, São Paulo 09210-580, Brazil*
(Dated: August 26, 2022)

The development of electronic devices based on the functionalization of (nano)cellulose platforms relies upon an atomistic understanding of the structural, and electronic properties of the combined system, cellulose/functional element. In this work, we present a theoretical study of the nanocellulose/graphene interface (nCL/G) based on first-principles calculations. We find that the binding energies of both hydrophobic/G (nCL^{phob}/G) and hydrophilic/G (nCL^{phil}/G) interfaces are primarily dictated by the van der Waals interactions, and are comparable with that of their 2D interface counterparts. We verify that the energetic preference of nCL^{phob}/G has been reinforced by the inclusion of an aqueous media via the implicit solvation model. Further structural characterization was carried out using a set of simulations of Carbon K-edge X-ray absorption spectra to identify and distinguish the key absorption features of the nCL^{phob}/G and nCL^{phil}/G interfaces. The electronic structure calculations reveal that the linear energy bands of graphene lie in the band gap of the nCL sheet, while depletion/accumulation charge density regions are observed. We show that external agents, i.e. electric field and mechanical strain, allow for tunability of the Dirac cone and the charge density at the interface. The control/maintenance of the Dirac cone states in nCL/G is an important feature for the development of electronic devices based on cellulosic platforms.

I. INTRODUCTION

Designing new biodegradable electronic devices based on renewable and environmentally sustainable platforms has been intensively investigated with the motivation to combat resource constraints and waste disposal challenges [1]. Most electronics are still assembled from non-renewable and nonbiodegradable materials and occasionally use production techniques that rely on hazardous compounds.

The possibility of building flexible devices using paper has led to the development of novel green electronic alternatives [2–4]. Cellulosic substrates have been explored for many applications, including transistors [5], supercapacitors [6], and organic solar cells [7]. More recently, nanoparticles extracted from cellulose pulps (cellulose nanocrystals-CNC and cellulose nanofibers-CNF) have also been considered lightweight and robust materials for electronic devices [8, 9]. Substrates produced from CNCs and CNFs display advantages over regular paper, including smoothness, high optical transparency, and superior mechanical properties [10, 11]. Besides, due to relatively inexpensive isolation methods, nanocellulose has excellent potential as a sustainable nanomaterial for designing many functional structures.

To impart electrical conductivity to cellulose, metallic particles [12], conductive polymers [13], carbon-based particles [14], and 2D materials [15] are usually integrated into nanocellulose through different techniques (coating, dipping, printing, blending, etc.). The combination of nanocellulose and 2D nanomaterials such as graphene, MoS$_2$, and MXene has recently triggered great interest in the scientific community as a new class of multifunctional hybrid compounds. By assembling graphene and nanocellulose within a stretchable elastomer matrix, Weng et al. [16] fabricated a robust strain sensor for efficient human-motion detection. Moisture-responsive foldable actuators were also produced from exfoliated graphene and amphiphilic nanocellulose by a simple vacuum filtration method [17]. Tian et al. [18] combined the excellent mechanical properties of CNF with the metal-like electrical conductivity of MXenes to design supercapacitor electrodes with high electronic conductivity of 2.95×10^4 S m^{-1}.

For electronic applications, 2D/nanocellulose hybrid materials should be able to tolerate mechanical stress and deformations while maintaining the satisfactorily electrical conductivity of 2D materials. Therefore, fundamental understanding of how the insertion of cellulose, a dielectric compound, influences the electrical properties of 2D materials is essential to guide the development of (nano) devices. Considerable experimental works on 2D/nanocellulose hybrids have shown promising outcomes. However, they only focus on the global electrical response and ignore the effect of nanocellulose/2D interaction at the nano and atomic levels on the electronic properties. Our group recently used first-principles calculations with a machine learning approach to evaluate relevant chemical and structural parameters that govern the binding energy of graphene oxide/nanocellulose interfaces [19], which have been considered promising polymeric composites for gas barriers [20] and water decontamination [21]. In the same direction, Zhu et al. [22] employed first-principles methods to study the interface

bonding behavior of graphene oxide and cellulose derivatives composite systems. Despite such previous studies, a detailed picture of the interaction between the different cellulose surfaces and graphene is hitherto unexplored.

In the current study, based on first-principles calculations, we investigate the (i) energetic stability, (ii) structural, and (iii) electronic properties of the nanocellulose/graphene interface (nCL/G). The hydrophobic (nCL^{phob}/G) and hydrophilic (nCL^{phil}/G) interfaces were addressed in this study. In (i), we have examined the role played by the vdW interaction on the nanocellulose - graphene binding strength and the aqueous media effect on the nCL/G binding energy. The structural characterization [(ii)] was performed by a set of X-ray near edge absorption structure (XANES) simulations of the nCL^{phob}/G and nCL^{phil}/G interfaces to identify the corresponding X-ray fingerprints. In (iii), we show that the Dirac bands of graphene lie in the nCL's bandgap, with the Dirac point at about 2 eV above the valence band maximum of the nanocellulose (ΔE_{DP}), followed by a small net charge transfer ($\Delta\rho \propto 10^{12} e/\text{cm}^2$) from graphene to the nCL/G interface region. In the sequence, we investigate the role of external agents such as electric field and mechanical strain in the electronic properties of nCL/G.

II. COMPUTATIONAL DETAILS

All calculations were performed within the density functional theory (DFT), where the exchange-correlation term was described by the generalized gradient approximation (GGA-PBE) [23] proposed by Perdew, Burke and Ernzerhof. The periodic image interaction was avoided by using at least 25 Å vacuum perpendicular to graphene sheet. The Kohn-Sham orbitals were expanded in a plane wave basis set with an energy cutoff of 400 eV and the electron-ion interaction have been evaluated using the PAW (projected augmented wave) method [24]. The Brillouin Zone (BZ) sampling was performed according to the Monkhorst-Pack scheme [25], using a $6\times6\times1$ mesh. The search for binding energies, equilibrium geometry and electronic properties were performed using Vienna Ab-initio Simulation Package (VASP) [26, 27], and the influence of an aqueous environment was simulated based on the implicit solvation model implemented in DFT code VASP (VASPsol [28–30]). The equilibrium configuration was calculated taken in account a fully relaxed of atomic positions, considering a convergence criteria of $25\,\text{meV/Å}$ for the atomic forces. In order to provide a more complete picture of the energetic features of the nCL/G interfaces, we have examined role played by the vdW dispersion interaction on the nCL/G binding energies. We have considered two different non-local vdW approaches, viz.: vdW-DF [31–33], and vdW-optB86b [34, 35].

The Carbon K-edge X-ray absorption near edge structure (XANES) spectra were simulated using XSpectra package [36–38], implemented in Quantum ESPRESSO
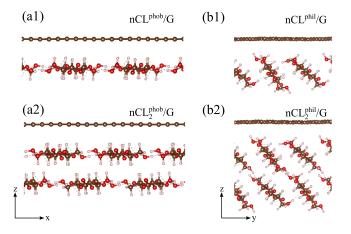

FIG. 1. Structural models of graphene interacting with the hydrophobic (a1)-(a2), and hydrophilic (b1)-(b2) nanocellulose sheet described by a single layer (a1)-(b1), and bilayer (a2)-(b2) of cellulose nanofibrils.

[39, 40]. To describe the K-edge spectra, we used a reconstructed ultrasoft pseudopotential with a core-hole in C-$1s$ orbital and the electron wave functions were recovered using GIPAW [41] reconstruction. Here, the BZ sampling was the same previously described and the energy cutoffs for the plane wave basis set and self-consistent total charge density were respectively 48 and 192 Ry.

III. RESULTS

The structural models of nCL/G interface are depicted in Fig. 1. The graphene layer interacts with the hydrophobic and hydrophilic nanocellulose sheets described by a single layer of cellulose fibrils, labelled as nCL^{phob}/G and nCL^{phil}/G in Fig. 1(a1) and (b1), and bilayer of cellulose fibrils, $\text{nCL}_2^{\text{phob}}$/G and $\text{nCL}_2^{\text{phil}}$/G in Fig. 1(a2) and (b2).

A. nCL/G Binding Energy and Geometry

We start our investigation by examining the energetic stability and equilibrium geometry of the nCL/G interface, and the role played by the long-range vdW forces on the nanocellulose - graphene binding strength. The hydrophobic interface is characterized by the predominance of CH-π bonds, whereas in nCL^{phil}/G the interface interaction is mainly dictated by the OH-π bonds. The nCL/G interface binding energy (E^b) was calculated by comparing the total energy of the final system ($E[\text{nCL/G}]$) and the sum to the total energies of the isolated components; for example, in Figs. 1(a1) and (b1) a single sheet of celulose nanofibrils ($E[\text{nCL}]$) and single layer graphene ($E[\text{G}]$),

$$E^b = E[\text{nCL/G}] - E[\text{nCL}] - E[\text{G}]. \qquad (1)$$

2

TABLE I. Binding energies (E^b in meV/Å^2) and the averaged ncl–G vertical distance (h in Å) of the nCL$^{\text{phob}}$/G and nCL$^{\text{phil}}$/G interfaces.

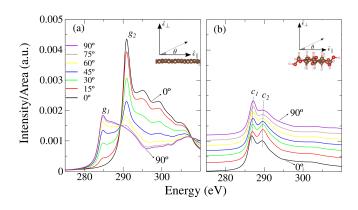|	nCL$^{\text{phob}}$/G		nCL$^{\text{phil}}$/G	
vdW	E^b	h	E^b	h
DF	12.92	2.71	11.63	2.59
optB86b	15.10	2.53	13.87	2.13
no vdW	0.51	3.04	0.81	2.90
DF-solvent	11.80	2.71	9.51	2.70
	nCL$_2^{\text{phob}}$/G		nCL$_2^{\text{phil}}$/G	
vdW	E^b	h	E^b	h
DF	13.22	2.75	12.34	2.51
optB86b	16.07	2.46	13.91	2.32
DF-solvent	12.92	2.74	9.69	2.69

FIG. 2. Carbon K-edge simulated XANES spectra of pristine graphene (a), and single layer cellulose fibrils (b) as a function of the radiation polarization angle (θ).

For each interface, i.e. nCL$^{\text{phob}}$/G and nCL$^{\text{phil}}$/G, we have considered three different stacking geometries. We found that E^b and the (averaged) equilibrium vertical distance between the nCL and graphene sheet (h) change by less than 0.06 meV/Å^2 and 0.01 Å.

Our results of E^b and h, summarized in Table I, reveal an energetic preference for the nCL$^{\text{phob}}$/G interface. By using the vdW-DF approach to describe the long-range vdW interactions we found binding energies of 12.92 and 11.63 meV/Å^2 for nCL$^{\text{phob}}$/G and nCL$^{\text{phil}}$/G, respectively. Comparing with other layered 2D counterpart systems, we find that the nCL$^{\text{phob}}$/G binding energy is (i) comparable with that of boron-nitride/G bilayer ($\sim$12 meV/Å^2 [42]); (ii) about 13% smaller compared with the intersheet binding energy of nCL; [43] and (iii) between 16% and 40% higher when compared to graphene oxide (GO) and nCL$^{\text{phob}}$interface, depending on the oxygen concentration [19]. In order to verify the reliability of our results, we have also calculated the binding energies (i) by using another vdW functional (optB86b in Table I), and (ii) adding a second layer of cellulose nanofibrils, nCL$_2^{\text{phob}}$/G and nCL$_2^{\text{phil}}$/G, as depicted in Figs. 1(a2) and (b2), respectively. Our E^b results, Table I, confirm the energetic preference for the nCL$^{\text{phob}}$/G interface.

The energetic preference of the nCL$^{\text{phob}}$/G interface is in agreement with recent theoretical findings based on molecular dynamic simulations [44, 45]. Both studies indicate that the presence of trapped water molecules at the nCL/G interface reduces the binding energy; moreover in Ref. 44 the authors verified the exclusion of the water molecules from the nCL$^{\text{phob}}$/G interface. Indeed, by using the implicit solvation model [29, 30] we find a reduction of the interface binding energy [Eq. 1], $E^b = 12.92 \rightarrow 11.80$ meV/Å^2 in nCL$^{\text{phob}}$/G, and $11.63 \rightarrow 9.51$ meV/Å^2 in the nCL$^{\text{phil}}$/G interface, while the equilibrium geometries of the nCL/G interfaces are nearly the same as those obtained previously with no solvent effects. It is worth noting that the larger binding energy reduction in the latter is due to the hydrophilic nature of the interface, which is in agreement

with our results of solvation energies (E^s)[46], namely 2.87 and 10.77 meV/Å^2 in nCL$^{\text{phob}}$/G and nCL$^{\text{phil}}$/G, respectively, and 4.21 and 11.19 in the nanocellulose bilayer systems, nCL$_2^{\text{phob}}$/G and nCL$_2^{\text{phil}}$/G.

Long range vdW dispersion interaction plays an important role in the interchain and intersheet binding energy between the cellulose fibrils and nCL sheets, respectively [43, 47]. To quantify the role played by the vdW interaction on the nCL - G binding energy, we have calculated E^b by turning off the vdW contribution. In this case, the binding energy of the nCL$^{\text{phob}}$/G (nCL$^{\text{phil}}$/G) interface reduces to 0.51 (0.81) meV/Å^2, and the vertical distance h increases to 3.04 (2.90) Å. Thus, similarly to the intersheet binding energy in pristine nCL,[43] we can deduce that the non-covalent (vdW) interactions rules the formation of nCL/G interfaces.

B. Structural Characterization, XANES

Core-level spectroscopy is a powerful tool to provide the structural characterization of materials in an atomic scale based on the local electronic properties of the probed element. Currently, the combination of experimental X-ray absorption near edge structure (XANES) data and first-principles simulations has proven to be a highly successful strategy to understand the atomic structure of novel materials [37, 48–50]. In this subsection, we present XANES simulation results of the Carbon K-edge absorption spectra of nCL/G interfaces in order to find spectroscopic finger prints of the atomic structures of the nCL$^{\text{phob}}$/G and nCL$^{\text{phil}}$/G interfaces.

Let us start with the XANES of the pristine isolated systems, graphene and single layer nCL. In Fig. 2(a), we present the absorption spectra of graphene as a function of the orientation (θ) of the radiation polarization vector ($\hat{\epsilon}$), where we can identify the C-1$s \rightarrow \pi^*$ [$\rightarrow \sigma^*$] transition for $\hat{\epsilon} = \hat{\epsilon}_\perp$ ($\theta = 90°$) [$\hat{\epsilon} = \hat{\epsilon}_\parallel$ ($\theta = 0°$)]. The energy positions of these absorption peaks, around 285 and 292 eV, respectively, indicated as g_1 and g_2 in Fig. 2(a),

and the dependence of their intensities with the orientation of the polarization vector are in good agreement with the previous experimental findings [51, 52].

Experimental results of XANES spectra of cellulose [53, 54] indicate the presence of two absorption peaks, at 289.3 and 290.7 eV, both attributed to the C-1$s \to \pi^*$ transition, associated to the C–OH and C–H bonds, respectively. Those bonding structures are present in the single layer nCL, and, indeed, the respective absorption spectra are captured in our simulations. In Fig. 2(b), we show our results for a single-layer nCL sheet which are characterized by (i) two absorption peaks, denoted c_1 and c_2, lying at about 287 and 290 eV, and (ii) reduced angular dependency with the direction of the polarization vector compared to the one of graphene [Fig. 2(a)]. As shown in Fig. 2(b), the energy positions of c_1 and c_2 changes by 0.36 and 0.21 eV, respectively, for $\theta = 0 \to 90°$.[55] The absorption spectra in the nCL bulk phase (not shown) have a similar characteristic, with c_1 and c_2 shifted by $\sim +2$ eV, for example $c1$: $287 \to 289$ eV.

The XANES spectra of nCL^{phob}/G and nCL^{phil}/G interfaces are shown in Figs. 3(a) and (b). In both spectra we identify the C-1$s \to \pi^*$ and $\to \sigma^*$ absorption features from graphene for $\theta = 90°$ and $0°$, respectively. Between these two transitions energies, we can identify the following differences on the absorption features in nCL^{phob}/G and nCL^{phil}/G attributed to the nCL absorption spectra. (i) The presence of absorption peaks *1a* and *2a* [Fig. 3(a)] for $\theta = 0°$, while in the nCL^{phil}/G we find one absorption feature, *1b* in Fig. 3(b); (ii) the absorption peak *2b* at 287.5 eV is clearly visible in the nCL^{phil}/G interface for $\theta = 90°$, but it is attenuated in nCL^{phob}/G; and (iii) due to the tilted geometry of cellulose fibrils with respect to the graphene layer, the absorption spectra in nCL^{phil}/G are no longer symmetric for positive and negative values of radiation polarization angles. For instance, the absorption features for $\theta = +15°$ and $-15°$ (dot-dashed lines) present different intensities, as seen in Fig. 3(b).

Because the formation of nCL/G heterostruture is ruled by the vdW interactions, with no covalent bonds between the nCL sheet and the graphene layer, the nCL/G interfaces' absorption spectra are primarily determined by the superposition of the ones of isolated components. Indeed, the absorption spectra can be better understood by XANES computations of hypothetical structures, namely, an isolated single-layer graphene, and nCL sheet (both) constrained to the respective nCL/G interface equilibrium geometry. The XANES simulations of these constrained structures reveal that the features *1a* and *2a* in nCL^{phob}/G emerge from the superposition of the edge transitions in graphene with the absorption peaks *c1a* and *c2a* of the nCL, Figs. 3(a1) and (a2). Similarly, the absorption peak *1b* in nCL^{phil}/G results from the superposition of graphene edge absorption structure with the *c1b* peak of the tilted layer of cellulose fibrils, Figs. 3(b1) and (b2), and for $\theta = 90°$ the absorption feature *2b* is composed by the superposition of graphene near-edge structure with the absorption peak *c2b* of the
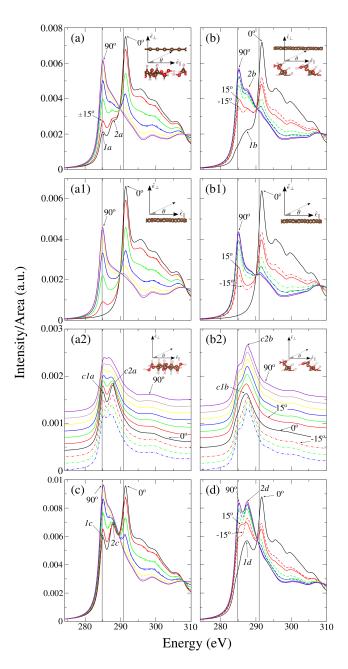

FIG. 3. XANES spectra of nCL^{phob}/G (a), and nCL^{phil}/G (b) interfaces. XANES spectra of hypothetical graphene [(a1)-(b1)] and single layer nCL sheet [(a2)-(b2)] constrained to the equilibrium geometry of the respective final system, nCL^{phob}/G and nCL^{phil}/G, as indicated in the insets. XANES spectra of nCL$_3^{phob}$/G (c), and nCL$_3^{phil}$/G (d).

tilted nCL.

The absorption spectra of the nCL/G systems, Figs. 3(a) and (b), were calculated by considering graphene on a single layer of cellulose sheet. However, when the number of nCL sheets grows, it is worthwhile to examine the changes on the XANES spectra. Our results reveal that as the number of nCL layers increases, the absorption characteristics from the C - H and
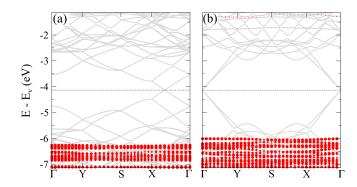
FIG. 4. Electronic band structure of nCL$^{\text{phob}}$/G (a) and nCL$^{\text{phil}}$/G (b). The zero energy was set at the vacuum level, the Fermi level is indicated by the dashed black lines, and red circles indicates cellulose contribution in band.

C-OH bonds grow more pronounced between 285 and 292 eV. In Fig. 3(c) and (d) we present the absorption spectra for three layer of cellulose fibrils, nCL$_3^{\text{phob}}$/G and nCL$_3^{\text{phil}}$/G. In the former interface the absorption peaks *1a* and *2a* become more apparent [labelled as *1c* and *2c* in Fig. 3(c)], similarly the features *1b* and *2b* of nCL$^{\text{phil}}$/G become more intense in nCL$_3^{\text{phil}}$/G, indicated as *1d* and *2d* in Fig. 3(d), and thus reinforcing the differences in the XANES signatures of the hydrophobic and hydrophilic nCL/G interfaces.

C. Electronic properties

The electronic properties of nCL/G are characterized by an insulator/semi-metal interface with the linear energy bands of graphene lying within the bandgap of nCL. In Figs. 4(a) and (b), we present the orbital projected electronic band structures of nCL$^{\text{phob}}$/G and nCL$^{\text{phil}}$/G, where we find (i) the graphene's Dirac-point (DP) at about 2 eV above the valence band maximum (VBM) of the nCL layer; and (ii) the emergence of an energy gap of $\sim$0.04 eV at the DP. There is a small amount of charge accumulation at the nCL/G interface. Based on the Bader analysis [56], we found a net charge transfer ($\Delta\rho$) of 0.23 (0.28) $\times 10^{13}$ e/cm^2 from graphene to the nCL$^{\text{phob}}$/G, (nCL$^{\text{phil}}$/G) interface, followed by a reduction of the graphene work-function (Φ)[57] by 0.2 eV compared with that of free-stading graphene sheet, $4.33 \rightarrow 4.13$ eV. Similar results were obtained in the nCL$_2^{\text{phob}}$/G and nCL$_2^{\text{phil}}$/G interfaces.

In Figs. 5(a) an (b) we present a map of the charge accumulations in the nCL$^{\text{phob}}$/G and nCL$^{\text{phil}}$/G interfaces, where the following characteristics are noteworthy: (i) the inhomogeneous (net) charge distribution on the graphene sheets [Figs. 5(a1) and (b1)], which can be attributed to the differences in the orbital hopping between the nCL surface and the graphene's π orbitals; and (ii), as depicted in Figs. 5(a2) and (b2), those charge transfers occurs primarily at the nCL/G interface, since $\Delta\rho \approx 0$ in
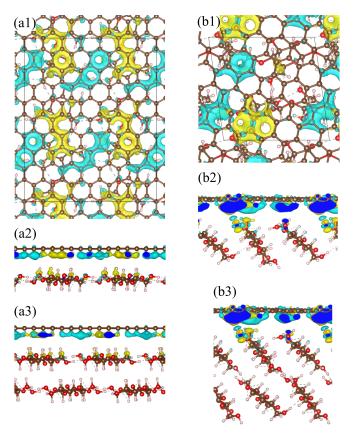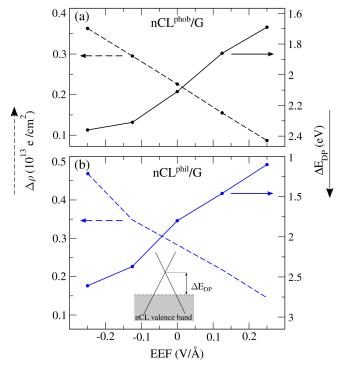

FIG. 5. Net charge tranfers, $\Delta\rho$ in nCL$^{\text{phob}}$/G (a1), nCL$^{\text{phil}}$/G (b1), nCL$_2^{\text{phob}}$/G (a2), and nCL$_2^{\text{phil}}$/G (b2). Isosurfaces of 0.4 me/Å^3, and postive (negative) values of $\Delta\rho$ are indicated in blue (yellow).

the subsurface nCL layers, Figs. 5(a3) and (b3). Such a net charge localization suggest the emergence of localized electronic transmission channels at the nCL/G interface. On the other hand, it is worth mentioning that such an inhomogeneous net charge distribution [(i)], giving rise to electron- and hole-rich regions in graphene, will play a deleterious role on the electronic transport properties throughout the nCL/G layers.

The understanding of the electronic properties of the nCL/G interface in the presence of external agents is an important issue for the development of electronic devices/sensors based on a combination of cellulosic materials and graphene. Thus, in the sequence, we will focus on the effects of external electric field (EEF) and mechanical compressive strain in the nCL/G interface.

Let us start with the effect of EEF.[58] As shown in Fig. 6, the energy position of the Dirac point with respect to the VBM of the nCL (ΔE_{DP}) increases from 1.6 (1.1) to 2.3 (2.6) eV in nCL$^{\text{phob}}$/G (nCL$^{\text{phil}}$/G), for EEF of -0.25 and $+0.25$ V/Å, respectively. Concomitantly, the G$\rightarrow$nCL/G net charge transfer, $\Delta\rho$, varies from 0.08 (0.14) to 0.36 (0.47) $\times 10^{13}$ e/cm^2. Such tuning of ΔE_{DP} and $\Delta\rho$ is nearly linear with respect to the EEF. In particular, for ΔE_{DP} as a function of the EEF we find the following rates, -1.43 eV/(V/Å) and -3.14 eV/(V/Å) in
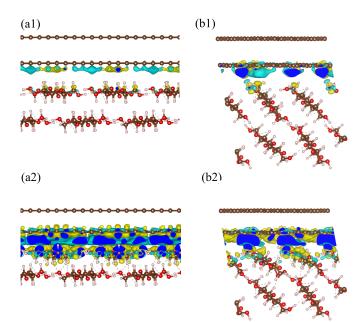
FIG. 6. Energy position of the DP with respect to the VBM (ΔE_{DP} - filled lines), and the net charge transfer from graphene to the nCL ($\Delta\rho$ in $10^{13}\,e/cm^2$ - dashed lines) as a function of the external electric field (EEF) for the nCL^{phob}/G (a), and nCL^{phil}/B (b) interfaces.

nCL^{phob}/G and nCL^{phil}/G, respectively. Assuming that such a linear relationship is preserved for larger values of EEF, we can infer that in nCL^{phil}/G the DP becomes resonant with the nCL valence band for EEF $> 0.6\,V/Å$, and thus suppressing the G $\to$ nCL/G charge transfer.

Further control of the electronic properties of 2D systems can be achieved through mechanical strain, "straintronics" [59, 60]. Indeed, such an approach has been used to control the electronic doping level in bilayer graphene and boron-nitride/graphene vdW heterostructures [61–63]. In nCL/G, the compressive strain will promote the strengthening the CH-π (OH-π) orbital overlap at the nCL^{phob}/G (nCL^{phil}/G) interface. Here, we investigate the net charge transfer, $\Delta\rho$, and the work function (Φ) in nCL/G, as a function of compressive strain. The strain in the nCL^{phob}/G and nCL^{phil}/G interfaces was applied by considering bilayers of nCL and graphene, nCL$_2^{phob}$/GBL [Fig. 7(a)] and nCL$_2^{phil}$/GBL [Fig. 7(b)]. In Figs. 7(a1) and (a2) we present the spatial distribution of $\Delta\rho$ of pristine nCL$_2^{phob}$/GBL and compressed by 9 %, respectively; similarly in Figs. 7(b1) and (b2), we present $\Delta\rho$ for the hydrofilic interface, nCL$_2^{phil}$/GBL. Interestingly, these $\Delta\rho$ maps reveal that the charge transfers are localized at the nCL$_2$/GBL interface region, and as shown in Figs. 8, the net charge transfer from G to the nCL increases up to ~ 1.0 (~ 0.8) $\times 10^{13}\,e/cm^2$ in nCL$_2^{phob}$/GBL (nCL$_2^{phil}$/GBL) for

FIG. 7. Side view of differential charge densities of nCL$_2^{phob}$/GBL (a) to 9% z-compressed nCL$_2^{phob}$/GBL (b), and nCL$_2^{phil}$/GBL (c) to 9% z-compressed nCL$_2^{phil}$/GBL (d). Isosurfaces of 0.4 me/Å^3

a compressive strain of about 9 %, which corresponds to an external pressure of 3.73 (3.15) GPa. Concomitantly with the G $\to$ nCL/G net charge transfer, we find slight increase of the work functions, namely from 4.64 (4.68) to 4.73 (4.88) eV in nCL$_2^{phil}$/GBL (nCL$_2^{phob}$/GBL) [Fig. 8]. Finally, we found that we can reach a p-type doping of about 1.1 (1.3) $\times 10^{13}\,e/cm^2$ of graphene upon an EEF of $-0.25\,V/Å$ in the 9% compressed nCL^{phob}/G (nCL^{phil}/G) interfaces. Thus, suggesting that suitable combinations of these external agents can be exploited to further modify the electrical characteristics of the nCL/G interface.

IV. SUMMARY AND CONCLUSIONS

We have performed a theoretical investigation of the energetic, structural, and electronic properties of nanocellulose/graphene (nCL/G) interface, where we have addressed the hydrophobic (nCL^{phob}/G) and hydrophilic (nCL^{phil}/G) interfaces. We find that the binding energy of nCL/G is primarily ruled by the vdW interactions, being comparable with that of boron-nitride/graphene. The structural fingerprints of nCL^{phob}/G and nCL^{phil}/G interfaces were identified through a detailed study of the Carbon K-edge absorption (XANES) spectra. The electronic structure of nCL/G is characterized by linear energy bands of graphene lying within the bandgap of nCL, with the Dirac point at about 2 eV above the valence band maximum of the nCL sheet, $\Delta E_{DP} \approx 2\,eV$, and a net charge

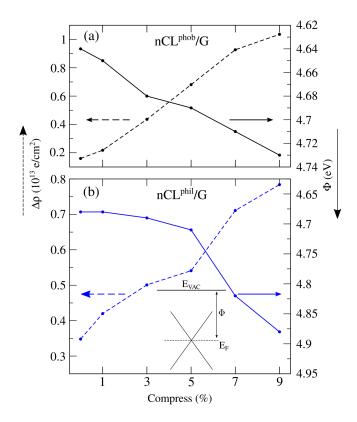FIG. 8. Net charge tranfer, $\Delta\rho$, and the work function Φ upon compression of nCL_2^{phob}/GBL (a) and nCL_2^{phil}/GBL (b). E_{vac} represents the vacuum level.

accumulation, $\Delta\rho$ of $\sim 0.2 \times 10^{13} e/cm^2$, localized at the nCL/G interface. External electric fields (EEFs) and mechanical strain were used to investigate the tunability of these quantities, where we found that ΔE_{DP} varies from 1.6 (1.1) to 2.3 (2.6) eV in nCL^{phob}/G (nCL^{phil}/G), for EEF of -0.25 and $+0.25\,V/\text{Å}$, respectively; whereas there is an increase of $G \rightarrow nCL/G$ $\Delta\rho$ up to $1 \times 10^{13} e/cm^2$ upon an external pressure of $3.73\,GPa$. We believe that our findings provide not only the energetic and atomic scale structural understanding of the nCL/G interface, but also a set of important information of the electronic properties to the development of electronic devices based on the combination of nanocellulose and graphene.

[1] Mihai Irimia-Vladu, ""Green" electronics: biodegradable and biocompatible materials and devices for sustainable future," Chem. Soc. Rev. **43**, 588–610 (2014).

[2] Hongli Zhu, Wei Luo, Peter N. Ciesielski, Zhiqiang Fang, J. Y. Zhu, Gunnar Henriksson, Michael E. Himmel, and Liangbing Hu, "Wood-Derived Materials for Green Electronics, Biological Devices, and Energy Applications," Chemical Reviews **116**, 9305–9374 (2016).

[3] Bin Yao, Jing Zhang, Tianyi Kou, Yu Song, Tianyu Liu, and Yat Li, "Paper-Based Electrodes for Flexible Energy Storage Devices," Advanced Science **4**, 1700107 (2017).

[4] Dawei Zhao, Ying Zhu, Wanke Cheng, Wenshuai Chen, Yiqiang Wu, and Haipeng Yu, "Cellulose-Based Flexible Functional Materials for Emerging Intelligent Electronics," Advanced Materials **33**, 2000619 (2021).

[5] Silvia Conti, Lorenzo Pimpolari, Gabriele Calabrese, Robyn Worsley, Subimal Majee, Dmitry K. Polyushkin, Matthias Paur, Simona Pace, Dong Hoon Keum, Filippo Fabbri, Giuseppe Iannaccone, Massimo Macucci, Camilla Coletti, Thomas Mueller, Cinzia Casiraghi, and Gianluca Fiori, "Low-voltage 2D materials-based printed field-effect transistors for integrated digital and analog electronics on paper," Nature Communications **11**, 3566 (2020).

[6] Zhe Gui, Hongli Zhu, Eleanor Gillette, Xiaogang Han, Gary W. Rubloff, Liangbing Hu, and Sang Bok Lee, "Natural Cellulose Fiber as Substrate for Supercapacitor," ACS Nano **7**, 6037–6046 (2013).

[7] Francesca Brunetti, Alessandra Operamolla, Sergio Castro-Hermosa, Giulia Lucarelli, Valerio Manca, Gianluca M. Farinola, and Thomas M. Brown, "Printed Solar Cells and Energy Storage Devices on Paper Substrates," Advanced Functional Materials **29**, 1806798 (2019).

[8] Xu Du, Zhe Zhang, Wei Liu, and Yulin Deng, "Nanocellulose-based conductive materials and their emerging applications in energy devices - A review," Nano Energy **35**, 299–320 (2017).

[9] Fanny Hoeng, Aurore Denneulin, and Julien Bras, "Use of nanocellulose in printed electronics: a review," Nanoscale **8**, 13131–13154 (2016).

[10] Robert J. Moon, Ashlie Martini, John Nairn, John Simonsen, and Jeff Youngblood, "Cellulose nanomaterials review: structure, properties and nanocomposites," Chem. Soc. Rev. **40**, 3941–3994 (2011).

[11] Carlos Salas, Tiina Nypelö, Carlos Rodriguez-Abreu, Carlos Carrillo, and Orlando J. Rojas, "Nanocellulose properties and applications in colloids and interfaces," Current Opinion in Colloid & Interface Science **19**, 383–396 (2014).

[12] Tetsuji Inui, Hirotaka Koga, Masaya Nogi, Natsuki Komoda, and Katsuaki Suganuma, "A Miniaturized Flexible Antenna Printed on a High Dielectric Constant Nanopaper Composite," Advanced Materials **27**, 1112–1116 (2015).

[13] Xuan Yang, Kaiyuan Shi, Igor Zhitomirsky, and Emily D. Cranston, "Cellulose Nanocrystal Aerogels as Universal 3D Lightweight Substrates for Supercapacitor Materials," Advanced Materials **27**, 6104–6109 (2015).

[14] Ana C. Fingolo, Vitória B. de Morais, Saionara V. Costa, Cátia C. Corrêa, Beatriz Lodi, Murilo Santhiago, Juliana S. Bernardes, and Carlos C. B. Bufon, "Enhanced Hydrophobicity in Nanocellulose-Based Materials: Toward Green Wearable Devices," ACS Applied Bio Materials **4**, 6682–6689 (2021).

[15] Shaomei Cao, Liyi Shi, Miao Miao, Jianhui Fang, Hongbin Zhao, and Xin Feng, "Solution-processed flexible paper-electrode for lithium-ion batteries based on MoS2 nanosheets exfoliated with cellulose nanofibrils," Electrochimica Acta **298**, 22–30 (2019).

[16] Zhe Weng, Yang Su, Da-Wei Wang, Feng Li, Jinhong Du, and Hui-Ming Cheng, "Graphene–Cellulose Paper Flexible Supercapacitors," Advanced Energy Materials **1**, 917–922 (2011).

[17] Xuezhu Xu and You-Lo Hsieh, "Aqueous exfoliated graphene by amphiphilic nanocellulose and its application in moisture-responsive foldable actuators," Nanoscale **11**, 11719–11729 (2019).

[18] Weiqian Tian, Armin VahidMohammadi, Michael S. Reid, Zhen Wang, Liangqi Ouyang, Johan Erlandsson, Torbjörn Pettersson, Lars Wågberg, Majid Beidaghi, and Mahiar M. Hamedi, "Multifunctional Nanocomposites with High Strength and Capacitance Using 2D MXene and 1D Nanocellulose," Advanced Materials **31**, 1902977 (2019).

[19] Romana Petry, Gustavo H. Silvestre, Bruno Focassio, Felipe Crasto de Lima, Roberto H. Miwa, and Adalberto Fazzio, "Machine Learning of Microscopic Ingredients for Graphene Oxide/Cellulose Interaction," Langmuir **38**, 1124–1130 (2022).

[20] Hanieh Mianehrow, Giada Lo Re, Federico Carosio, Alberto Fina, Per Tomas Larsson, Pan Chen, and Lars A. Berglund, "Strong reinforcement effects in 2D cellulose nanofibril–graphene oxide (CNF–GO) nanocomposites due to GO-induced CNF ordering," J. Mater. Chem. A **8**, 17608–17620 (2020).

[21] Chuantao Zhu, Peng Liu, and Aji P. Mathew, "Self-Assembled TEMPO Cellulose Nanofibers: Graphene Oxide-Based Biohybrids for Water Purification," ACS Applied Materials & Interfaces **9**, 21048–21058 (2017).

[22] Bowen Zhu, Kexuan Wang, Weisheng Sun, Ziyan Fu, Hassan Ahmad, Mizi Fan, and Haili Gao, "Revealing the adsorption energy and interface characteristic of cellulose-graphene oxide composites by first-principles calculations," Composites Science and Technology **218**, 109209 (2022).

[23] John P. Perdew, Kieron Burke, and Matthias Ernzerhof, "Generalized Gradient Approximation Made Simple," Phys. Rev. Lett. **77**, 3865–3868 (1996).

[24] P. E. Blöchl, "Projector augmented-wave method," Phys. Rev. B **50**, 17953–17979 (1994).

[25] Hendrik J. Monkhorst and James D. Pack, "Special points for Brillouin-zone integrations," Phys. Rev. B **13**, 5188–5192 (1976).

[26] G. Kresse and J. Furthmüller, "Efficiency of ab-initio total energy calculations for metals and semiconductors using a plane-wave basis set," Computational Materials Science **6**, 15–50 (1996).

[27] G. Kresse and J. Furthmüller, "Efficient iterative schemes for ab initio total-energy calculations using a plane-wave basis set," Phys. Rev. B **54**, 11169–11186 (1996).

[28] K. Mathew, V. S. Chaitanya Kolluru, and R. G. Hennig, "VASPsol: Implicit solvation and electrolyte model for density-functional theory," GitHub repository (2018), 10.5281/zenodo.2555053.

[29] Kiran Mathew, Ravishankar Sundararaman, Kendra Letchworth-Weaver, T. A. Arias, and Richard G. Hennig, "Implicit solvation model for density-functional study of nanocrystal surfaces and reaction pathways," The Journal of Chemical Physics **140**, 084106 (2014).

[30] Kiran Mathew, V. S. Chaitanya Kolluru, Srinidhi Mula, Stephan N. Steinmann, and Richard G. Hennig, "Implicit self-consistent electrolyte model in plane-wave density-functional theory," The Journal of Chemical Physics **151**, 234101 (2019).

[31] T. Thonhauser, S. Zuluaga, C. A. Arter, K. Berland, E. Schröder, and P. Hyldgaard, "Spin Signature of Nonlocal Correlation Binding in Metal-Organic Frameworks," Phys. Rev. Lett. **115**, 136402 (2015).

[32] T. Thonhauser, Valentino R. Cooper, Shen Li, Aaron Puzder, Per Hyldgaard, and David C. Langreth, "Van der Waals density functional: Self-consistent potential and the nature of the van der Waals bond," Phys. Rev. B **76**, 125112 (2007).

[33] D C Langreth, B I Lundqvist, S D Chakarova-Käck, V R Cooper, M Dion, P Hyldgaard, A Kelkkanen, J Kleis, Lingzhu Kong, Shen Li, P G Moses, E Murray, A Puzder, H Rydberg, E Schröder, and T Thonhauser, "A density functional for sparse matter," Journal of Physics: Condensed Matter **21**, 084203 (2009).

[34] Jiří Klimeš, David R Bowler, and Angelos Michaelides, "Chemical accuracy for the van der Waals density functional," Journal of Physics: Condensed Matter **22**, 022201 (2009).

[35] Ji ří Klimeš, David R. Bowler, and Angelos Michaelides, "Van der Waals density functionals applied to solids," Phys. Rev. B **83**, 195131 (2011).

[36] Oana Bunău and Matteo Calandra, ""projector augmented wave calculation of x-ray absorption spectra at the l2,3 edges"," Phys. Rev. B **87**, 205105 (2013).

[37] Christos Gougoussis, Matteo Calandra, Ari P. Seitsonen, and Francesco Mauri, "First-principles calculations of x-ray absorption in a scheme based on ultrasoft pseudopotentials: From α-quartz to high-T_c compounds," Phys. Rev. B **80**, 075102 (2009).

[38] Mathieu Taillefumier, Delphine Cabaret, Anne-Marie Flank, and Francesco Mauri, "X-ray absorption near-edge structure calculations with the pseudopotentials: Application to the K edge in diamond and α-quartz," Phys. Rev. B **66**, 195107 (2002).

[39] Paolo Giannozzi, Stefano Baroni, Nicola Bonini, Matteo Calandra, Roberto Car, Carlo Cavazzoni, Davide Ceresoli, Guido L Chiarotti, Matteo Cococcioni, Ismaila Dabo, Andrea Dal Corso, Stefano de Gironcoli, Stefano Fabris, Guido Fratesi, Ralph Gebauer, Uwe Gerstmann, Christos Gougoussis, Anton Kokalj, Michele Lazzeri, Layla Martin-Samos, Nicola Marzari, Francesco Mauri, Riccardo Mazzarello, Stefano Paolini, Alfredo Pasquarello, Lorenzo Paulatto, Carlo Sbraccia, Sandro Scandolo, Gabriele Sclauzero, Ari P Seitsonen, Alexander Smogunov, Paolo Umari, and Renata M Wentzcovitch, "QUANTUM ESPRESSO: a modular and open-source software project for quantum simulations of materials," Journal of Physics: Condensed Matter **21**, 395502 (2009).

[40] Kristian Berland, Valentino R Cooper, Kyuho Lee, Elsebeth Schröder, T Thonhauser, Per Hyldgaard, and Bengt I Lundqvist, "van der Waals forces in density functional theory: a review of the vdW-DF method," Reports on

Progress in Physics **78**, 066501 (2015).

[41] Chris J. Pickard and Francesco Mauri, "All-electron magnetic response with pseudopotentials: NMR chemical shifts," Phys. Rev. B **63**, 245101 (2001).

[42] Yingcai Fan, Mingwen Zhao, Zhenhai Wang, Xuejuan Zhang, and Hongyu Zhang, "Tunable electronic structures of graphene/boron nitride heterobilayers," Applied Physics Letters **98**, 083103 (2011).

[43] Gustavo H. Silvestre, Lidiane O. Pinto, Juliana S. Bernardes, Roberto H. Miwa, and Adalberto Fazzio, "Disassembly of TEMPO-Oxidized Cellulose Fibers: Intersheet and Interchain Interactions in the Isolation of Nanofibers and Unitary Chains," The Journal of Physical Chemistry B **125**, 3717–3724 (2021).

[44] Rasha Alqus, Stephen J. Eichhorn, and Richard A. Bryce, "Molecular Dynamics of Cellulose Amphiphilicity at the Graphene–Water Interface," Biomacromolecules **16**, 1771–1783 (2015).

[45] Hanieh Mianehrow, Lars A. Berglund, and Jakob Wohlert, "Interface effects from moisture in nanocomposites of 2D graphene oxide in cellulose nanofiber (CNF) matrix – A molecular dynamics study," J. Mater. Chem. A **10**, 2122–2132 (2022).

[46] E^s is defined as the diference between the vacuum total energy and solvent total energy.

[47] Yan Li, Milo Lin, and James W. Davenport, "Ab Initio Studies of Cellulose I: Crystal Structure, Intermolecular Forces, and Interactions with Water," The Journal of Physical Chemistry C **115**, 11533–11539 (2011).

[48] David Prendergast and Giulia Galli, "X-Ray Absorption Spectra of Water from First Principles Calculations," Phys. Rev. Lett. **96**, 215502 (2006).

[49] F. Crasto de Lima, A. Fazzio, A. B. McLean, and R. H. Miwa, "Simulations of X-ray absorption spectroscopy and energetic conformation of N-heterocyclic carbenes on Au(111)," Phys. Chem. Chem. Phys. **22**, 21504–21511 (2020).

[50] Alex Inayeh, Ryan R. K. Groome, Ishwar Singh, Alex J. Veinot, Felipe Crasto de Lima, Roberto H. Miwa, Cathleen M. Crudden, and Alastair B. McLean, "Self-assembly of N-heterocyclic carbenes on Au(111)," Nature Communications **12**, 4034 (2021).

[51] Theanne Schiros, Dennis Nordlund, Lucia Pálová, Deborah Prezzi, Liuyan Zhao, Keun Soo Kim, Ulrich Wurstbauer, Christopher Gutiérrez, Dean Delongchamp, Cherno Jaye, Daniel Fischer, Hirohito Ogasawara, Lars G. M. Pettersson, David R. Reichman, Philip Kim, Mark S. Hybertsen, and Abhay N. Pasupathy, "Connecting Dopant Bond Type with Electronic Structure in N-Doped Graphene," Nano Letters **12**, 4025–4031 (2012).

[52] Andreas Lippitz, Jörg F. Friedrich, and Wolfgang E.S. Unger, "Plasma bromination of HOPG surfaces: A NEXAFS and synchrotron XPS study," Surface Science **611**, L1–L7 (2013).

[53] George D. Cody, "Probing chemistry within the membrane structure of wood with soft X-ray spectral microscopy," (2000) pp. 307–312.

[54] Chithra Karunakaran, Colleen R Christensen, Cedric Gaillard, Rachid Lahlali, Lisa M Blair, Vijayan Perumal, Shea S Miller, and Adam P Hitchcock, "Introduction of soft X-ray spectromicroscopy as an advanced technique for plant biopolymers research," PloS one **10**, e0122959 (2015).

[55] The simulations of the XANES spectra of nCL were performed by taken into account the polar angle [θ, presented in Figs.2 and 3], and two azimuthal (ϕ) angles, one for polarization vectors parallel and another perpendicular to the cellulose fibrils.

[56] R. Bader, *Atoms in Molecules: A Quantum Theory* (Oxford University Press, New York, 1990).

[57] The work function, Φ, is defined as the energy position of the Fermi level with respect to the vacuum level, $\Phi = E_F - E_{vac}$, where E_{vac} is obtained from the electrostatic potential calculation in a vacuum region far away from the system. Here we set $E_{vac} = 0$.

[58] For each value of electric field, the atomic positions of the nCL^{phob}/G system were fully relaxed.

[59] Chen Si, Zhimei Sun, and Feng Liu, "Strain engineering of graphene: a review," Nanoscale **8**, 3207–3217 (2016).

[60] Feng Miao, Shi-Jun Liang, and Bin Cheng, "Straintronics with van der Waals materials," npj Quantum Materials **6**, 1–4 (2021).

[61] Matthew Yankowitz, K Watanabe, T Taniguchi, Pablo San-Jose, and Brian J LeRoy, "Pressure-induced commensurate stacking of graphene on boron nitride," Nature communications **7**, 1–8 (2016).

[62] Tom Vincent, Vishal Panchal, Tim Booth, Stephen R Power, Antti-Pekka Jauho, Vladimir Antonov, and Olga Kazakova, "Probing the nanoscale origin of strain and doping in graphene-hBN heterostructures," 2D Materials **6**, 015022 (2018).

[63] Alexis Forestier, Félix Balima, Colin Bousige, Gardênia de Sousa Pinheiro, Rémy Fulcrand, Martin Kalbáč, Denis Machon, and Alfonso San-Miguel, "Strain and Piezo-Doping Mismatch between Graphene Layers," The Journal of Physical Chemistry C **124**, 11193–11199 (2020).